Interaction of Yeast Iso-1-cytochrome *c* with Cytochrome *c* Peroxidase Investigated by [^{15}N,^{1}H] Heteronuclear NMR Spectroscopy†

Jonathan A. R. Worrall, Urszula Kolczak, Gerard W. Canters, and Marcellus Ubbink*

Gorlaeus Laboratories, Leiden Institute of Chemistry, Leiden University, P.O. Box 9502, 2300 RA Leiden, The Netherlands

Received November 8, 2000; Revised Manuscript Received March 14, 2001

ABSTRACT: The interaction of yeast iso-1-cytochrome *c* with its physiological redox partner cytochrome *c* peroxidase has been investigated using heteronuclear NMR techniques. Chemical shift perturbations for both ^{15}N and ^{1}H nuclei arising from the interaction of isotopically enriched ^{15}N cytochrome *c* with cytochrome *c* peroxidase have been observed. For the diamagnetic, ferrous cytochrome *c*, 34 amides are affected by binding, corresponding to residues at the front face of the protein and in agreement with the interface observed in the 1:1 crystal structure of the complex. In contrast, for the paramagnetic, ferric protein, 56 amides are affected, corresponding to residues both at the front and toward the rear of the protein. In addition, the chemical shift perturbations were larger for the ferric protein. Using experimentally observed pseudocontact shifts the magnetic susceptibility tensor of yeast iso-1-cytochrome *c* in both the free and bound forms has been calculated with H^N nuclei as inputs. In contrast to an earlier study, the results indicate that there is no change in the geometry of the magnetic axes for cytochrome *c* upon binding to cytochrome *c* peroxidase. This leads us to conclude that the additional effects observed for the ferric protein arise either from a difference in binding mode or from the more flexible overall structure causing a transmittance effect upon binding.

Protein−protein interactions are an important feature of a variety of biological processes (*1*). In general, protein−protein complexes can range from static to transient. Static complexes are characterized by a slow dissociation rate, and the partners in the complex usually bind strongly in a single well-defined orientation. In contrast, transient complexes form when a high turnover is required such as in ET[1] processes. In many cases the formation of ET protein complexes is influenced by long-range electrostatic interactions leading to the formation of an encounter complex. This encounter complex can then sample a number of orientations of approximately equal energy within the binding domain, with the optimal orientation for efficient ET being achieved by short-range forces such as hydrophobic contacts and H-bonds (*2*, *3*). These dynamic features of redox protein−protein interactions make the task of structure determination a difficult one, with six X-ray crystal structures of ET protein complexes having so far been characterized (*4*−*9*). Advances in heteronuclear NMR in combination with paramagnetic NMR spectroscopy offer new possibilities for studying redox protein complexes (*10*). With the use of heteronuclear NMR detailed information concerning the nature of the recognition sites in solution can be obtained, and along with paramagnetic restraints elucidation of the complex structure is possible (*11*−*13*). In this study we have investigated the protein recognition site of cyt *c* in solution upon complex formation with its physiological redox partner CcP using heteronuclear NMR spectroscopy.

Both proteins are located in the intermembrane space of yeast mitochondria, where CcP (34 kDa) catalyzes the two-electron reduction of alkyl hydroperoxides, utilizing two molecules of ferrous cyt *c* (12.5 kDa) as its specific electron source (*14*). The active sites of both proteins consist of a heme moiety. For cyt *c* the heme is covalently attached to the polypeptide chain through a Cys-X-X-Cys binding motif. The iron in both the ferric and ferrous oxidation state is six coordinate low spin (Fe^{III}, $S = {}^1/_2$; Fe^{II}, $S = 0$). Resting state CcP (Fe^{III}) contains a noncovalent heme with a five-coordinate, high-spin iron ($S = {}^5/_2$). Here, the sixth coordination position is vacant, allowing the peroxide substrate to bind. From the crystal structure of the 1:1 yeast cyt *c*:CcP complex (Figure 1), the interaction consists predominately of van der Waals forces and one hydrogen bond (*4*), rather than the predicted electrostatic interactions proposed in an earlier model (*16*). The presence of a second binding site on the surface of CcP for cyt *c* has been confirmed at physiological ionic strength using transient absorption spectroscopy (*17*, *18*). This second site is more efficient in ET but exhibits a lower binding affinity compared to the so-called high-affinity binding site proposed to be observed in the crystals (*14*, *17*, *18*). A recent report using site-directed mutagenesis on CcP has identified the location of this second site, but as of yet it is structurally undetermined (*19*). Direct characterization of the second binding site by NMR or X-ray crystallography will be especially challenging given its high (millimolar range) dissociation constant (*14*, *17*, *18*). Although the "static view" depicted in the crystal structure

† This work was supported by TMR Haemworks Contract FMRX-CT98-0218.

* To whom correspondence should be addressed. Phone: +31 71 527 4628. Fax: +31 71 527 4593. E-mail: m.ubbink@chem.leidenuniv.nl.

[1] Abbreviations: ET, electron transfer; cyt *c*, iso-1-cytochrome *c*; CcP, cytochrome *c* peroxidase; NMR, nuclear magnetic resonance; HSQC, heteronuclear single-quantum coherence.

10.1021/bi0025823 CCC: $20.00
Published on Web 05/24/2001

FIGURE 1: Crystal structure of the yeast cyt *c* (light):CcP (dark) complex taken from the PDB entry 2PCC and drawn with MOLSCRIPT (*15*). Heme groups are shown in ball-and-stick representation along with the intermolecular H-bond between Glu290 (CcP) and Asn70 (cyt *c*) observed in the crystals. Some other relevant interface residues are also shown in ball-and-stick representation.

provides an intriguing insight into the nature of this ET complex, theoretical and experimental evidence suggests that the 1:1 complex is more dynamic in solution (*20*−*23*). Moreover, the current picture postulates that the high-affinity site consists of a single domain with a continuum of binding sites and that the 1:1 crystal structure corresponds to one of these sites within the binding domain (*14*, *23*).

From an NMR perspective a number of homonuclear experiments and hydrogen/deuterium exchange labeling studies have unveiled invaluable information concerning this protein−protein interaction (*24*−*30*). An interesting observation from the two reported hydrogen/deuterium exchange studies is the species-specific preference by CcP for its partner (*28*, *29*), thus highlighting the importance of studying protein−protein interactions with the homologous physiological partners. However, the overall size of the protein complex (48 kDa) severely limits further study of the complex by homonuclear NMR methods. In this study we have used ^{15}N-labeled yeast cyt *c* expressed in *Escherichia coli* (*31*, *32*) to map the interaction site on both oxidized and reduced cyt *c* upon 1:1 complex formation to resting state CcP. Upon complex formation chemical shift perturbations of ^{15}N and ^{1}H nuclei of cyt *c* are observed in both oxidation states, allowing a direct comparison to be made of the binding site of cyt *c* in solution with the interface in the crystals. Interestingly, differences are noted in both the size of the chemical shift perturbations induced by binding and the surface areas affected in the two oxidation states of cyt *c*.

MATERIALS AND METHODS

Protein Preparation. Isotopically enriched ^{15}N yeast cyt *c* (C102T) and wild-type yeast CcP were expressed in *E. coli* and purified as previously described (*31*−*33*). Oxidized cyt *c* was prepared by addition of an excess (2−3-fold) of $K_3[Fe(CN)_6]$ followed by dialysis under nitrogen against 20 mM sodium phosphate, I = 100 mM (NaCl), pH 6.0, by ultrafiltration methods (Amicon; YM3 membrane). Reduced cyt *c* was prepared in an analogous way except sodium ascorbate was used as reductant. Crystals of yeast CcP (stored at −80 °C) were dissolved in 20 mM sodium phosphate, I = 100 mM (NaCl), pH 6.0, and concentrated to a required volume by ultrafiltration (Amicon; YM10 membrane). Protein concentrations for cyt *c* were determined spectrophotometrically according to the absorbance peaks at 410 nm (ϵ = 106.1 mM^{-1} cm^{-1}) for oxidized and 550 nm (ϵ = 27.5 mM^{-1} cm^{-1}) for reduced protein. Because of the reported aging process of CcP the optical absorbance spectra were carefully analyzed to confirm the presence of the resting state enzyme (*34*). The peak maximum at 408 nm (ϵ = 98.0 mM^{-1} cm^{-1}) was used for determination of concentration and peak ratios; $A_{408/280}$ (1.28), $A_{408/308}$ (1.57), and $A_{620/647}$ (0.76) at pH 6.0 were used as criteria for confirmation of the high-spin five-coordinate species (*34*).

NMR samples of ^{15}N cyt *c* contained 1−1.8 mM protein in 20 mM sodium phosphate, I = 100 mM (NaCl), pH 6.0, 6% D_2O, and 100 μM [^{15}N]acetamide ($CH_3CO^{15}NH_2$) as an internal reference. For the reduced protein 100 μM sodium ascorbate was also present to maintain a reducing environment. NMR samples of CcP were prepared in an identical manner to give a final concentration of resting state enzyme of 0.5 mM. The pH for both protein samples was adjusted to 6.00 ± 0.05, and the solutions were degassed with argon.

NMR Experiments. Measurements were performed on a Bruker Avance DMX600 spectrometer operating at 313 K. [^{15}N,^{1}H]-HSQC spectra were obtained with spectral widths of 40.5 ppm (^{15}N) and 17.9 ppm (^{1}H) for oxidized cyt *c* and 45.6 ppm (^{15}N) and 13.9 ppm (^{1}H) for reduced cyt *c*. Spectra were first recorded with free cyt *c* followed by a titration of cyt *c* to resting state CcP, giving a final protein ratio of 1:3 (CcP:cyt *c*). Titrations were performed for cyt *c* in both oxidation states, with the pH checked before and after each titration step. Data processing was performed in AZARA (available from ftp://ftp.bio.cam.ac.uk/pub/azara). Assignments of the ^{15}N, ^{1}H nuclei of free yeast cyt *c* in both oxidized and reduced forms were aided by known literature assignments (*35*, *36*). The amides which were unassigned in this work were F-4, A3, H33, G83, and G84 in both the oxidized and reduced forms of the protein and, in addition, K4 and K11 in the reduced form. Chemical shift perturbations of ^{15}N and ^{1}H nuclei for cyt *c* upon interaction with CcP were analyzed by overlaying the spectra of bound cyt *c* with the free protein in the assignment program Ansig (*37*, *38*).

Magnetic Axes Calculations. Experimental pseudocontact shifts (ps) were obtained for the free protein from

$$\delta_{ps}(\text{free}) = \delta_{obs}(\text{oxidized free}) - \delta_{obs}(\text{reduced free}) \quad (1)$$

and for the bound protein from

$$\delta_{ps}(\text{bound}) = \delta_{obs}(\text{oxidized bound}) - \delta_{obs}(\text{reduced bound}) \quad (2)$$

with the δ_{ps} described by the general equation (*39*, *40*)

$$\delta_{ps} = 1/(12\pi N_A)[\Delta\chi_{ax}G'_{ax} + 1.5\Delta\chi_{rh}G'_{rh}]\Gamma(\alpha, \beta, \gamma) \quad (3)$$

The axial and rhombic anisotropies, $\Delta\chi_{ax}$ and $\Delta\chi_{rh}$, respectively, are given as $\Delta\chi_{ax} = \chi_{zz} - 0.5(\chi_{xx} + \chi_{yy})$ and $\Delta\chi_{rh} = \chi_{xx} - \chi_{yy}$, where χ_{xx}, χ_{yy}, χ_{zz} are the principal components of

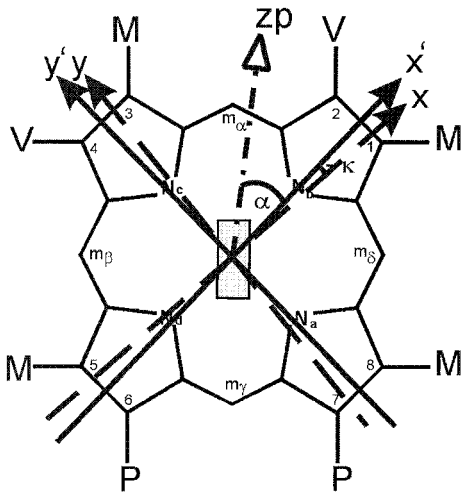

FIGURE 2: Schematic definition of the magnetic axes, *x*, *y*, *z*, in cyt *c* based on a pseudosymmetric iron-centered reference frame, *x*′, *y*′, *z*′, where *z*′ corresponds to the heme normal oriented toward the axial ligand His18 and *zp* is the projection of the *z* axis on the *x*′/*y*′ plane with respect to *x*′. The letters M, V, and P represent the vinyl, methyl, and propionate heme substituents, respectively.

the magnetic susceptibility tensor. The axial (G'_{ax}) and rhombic (G'_{rh}) geometric factors are described as

$$G'_{ax} = (3\cos^2\theta' - 1)R^{-3} \quad \text{and}$$
$$G'_{rh} = (\sin^2\theta' \cos 2\phi')R^{-3} \quad (4)$$

where R, θ', ϕ' (x', y', z') are the polar (Cartesian) coordinates of a nucleus in an arbitrary iron-centered coordinate system and $\Gamma(\alpha, \beta, \gamma)$ is the Euler rotation matrix that converts the arbitrary iron-centered coordinate system into the magnetic coordinate system R, θ, ϕ (x, y, z) (Figure 2). The β angle measures the deviation of z (χ_{zz}) from the heme normal defined by the Fe−N(His18) bond (z'), and α is defined as the angle between the projection of the z axis onto the x'/y' plane with respect to the x' axis (Figure 2). When β is small, $\kappa = \alpha + \gamma$, which represents the orientation of the χ_{xx} and χ_{yy} relative to the x' and y′ axes (Figure 2).

The arbitrary polar coordinates R, θ', ϕ' were determined using the X-ray crystal structures of free yeast cyt *c* (PDB entry 1YCC) (*41*) and yeast cyt *c* complexed to CcP (2PCC) (*4*). For this analysis the program MOLMOL (*42*) was used to add proton coordinates. The reference frame was defined as having the origin at the Fe, the z' axis perpendicular to the plane defined by the pyrrolic nitrogens, the x' axis lying along the N_d-N_b direction, and the y' axis lying along the N_a-N_c direction (Figure 2). All calculations were performed on both the free and bound crystal structure coordinates using the NMR data for free and bound cyt *c* obtained from eqs 1 and 2. The magnetic anisotropies, $\Delta\chi_{ax}$ and $\Delta\chi_{rh}$, and the Euler rotation angles (α, β, γ) were obtained from eq 3 by minimizing the following error function:

$$F = \sum(\delta_{ps}(\text{obs}) - \delta_{ps}(\text{cal}))^2 \quad (5)$$

where δ_{ps}(obs) is the difference of the chemical shifts between oxidized and reduced cyt *c* and δ_{ps}(cal) is calculated from eq 3. The residuals for the overall fits were defined as $F/(n-5)$, where n is the number of residues.

RESULTS

Chemical Shift Mapping of the Interaction Site on Ferrous and Ferric Cyt c. To analyze the interactions in solution of the complex formed between cyt *c* and CcP, [^{15}N,^{1}H]-HSQC spectra of free cyt *c* were recorded first, followed by a titration of ^{15}N cyt *c* to an initial 0.5 mM sample of resting state CcP at various cyt *c* concentrations (0.3−3 molar equiv). Experiments with both ferrous and ferric ^{15}N cyt *c* titrated to CcP were carried out. In both cases a general broadening of the resonances (Figure 3A) and significant chemical shift changes ($\Delta\delta_{binding}$) for the ^{15}N, ^{1}H nuclei of cyt *c* were observed, as illustrated in an overlay for a region of the [^{15}N,^{1}H]-HSQC spectra for free and bound ferrous cyt *c* in Figure 3B. The observed line broadening of the shifted peaks (8−15 Hz) is no larger than that of the unaffected peaks in the bound form. This behavior is characteristic of a fast exchange process on the NMR time scale, yielding a single averaged resonance for the perturbed cross-peak of cyt *c* upon complex formation to CcP. A lower limit for the rate of cyt *c* dissociation from the complex of 1200 s^{-1} is calculated and can be compared to a previous literature value of 1133 s^{-1} (*24*). However, as is pointed out by Satterlee and co-workers (*25*, *27*), these values must be interpreted with caution as the exchange kinetics in such a process are dependent on the complex concentration. Addition of excess cyt *c* caused the perturbed cross-peaks to move back toward the positions of the free form. This allowed titration curves to be plotted (Figure 3C) for individual perturbed resonances (*43*), and the derived lower limit for the binding constant (K_a) of 2×10^5 M^{-1} compares well with the reported value of $7-8 \times 10^5$ M^{-1} (*19*), indicating that >95% of cyt *c* is bound to CcP for a 1:1 stoichiometry with the protein concentrations used.

At equimolar concentrations the $\Delta\delta_{binding}$ for ferrous cyt *c* varies from −0.10 to 0.41 ppm for protons and from −0.60 to 0.74 ppm for nitrogens, with a total of 34 amides affected upon complex formation (Figure 4A and Table S1). For the ferric protein the $\Delta\delta_{binding}$ varies between −0.28 and 0.86 ppm for protons and between −1.43 and 1.45 ppm for nitrogens, with a total of 56 amides affected upon complex formation (Figure 4B and Table S2). From the NMR study of the nonphysiological complex between cyt *c* and plastocyanin (*43*) the size of the chemical shift changes observed for amide protons was relatively small, and it was concluded that this complex existed in a dynamic ensemble of structures. Here, the relatively large chemical shift changes suggest that cyt *c* occupies a single orientation for a significant fraction of the complex lifetime.

In Figure 5, the chemical shift changes for both oxidation states of cyt *c* have been mapped onto surface representations of the protein, with each residue colored according to increasing $\Delta\delta_{binding}$ for their amides using the color coding in Table 1. For ferrous cyt *c* the 34 affected amides are located solely on the front face of the protein, with the amides of Thr12, Gln16, and Phe82 demonstrating the greatest $\Delta\delta_{binding}$. For the ferric protein the majority of the 56 affected amides map onto the front face of cyt *c*, with the remaining affected ones located more toward the side and rear of the protein. The amides of Thr8, Thr12, Gln16, Val28, Asn70, and Asp90 have the greatest $\Delta\delta_{binding}$, and all lie on the front face of the protein. Except for the additional effects observed

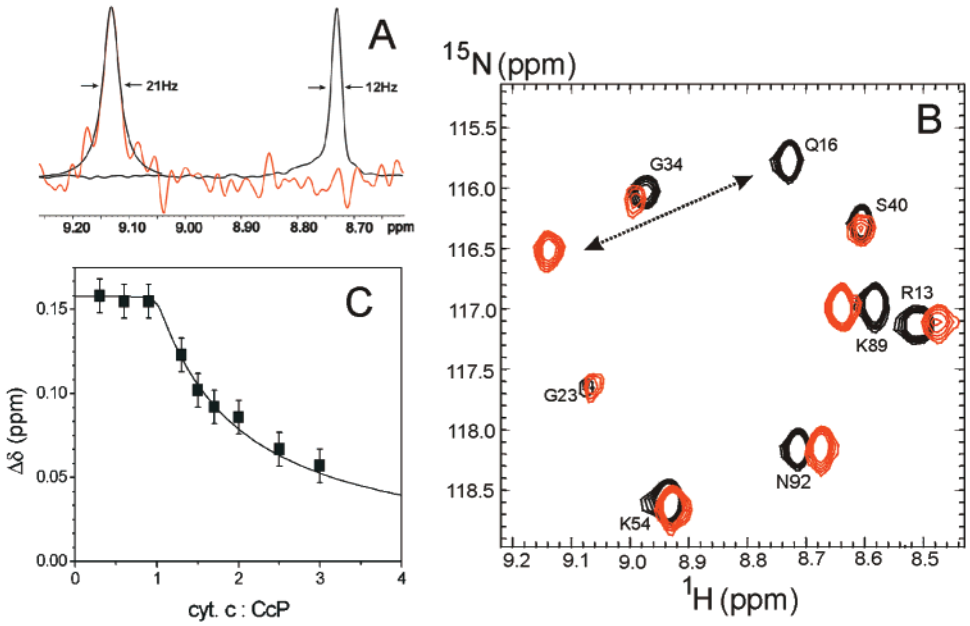

FIGURE 3: (A) 1D slice of the [^{15}N,^{1}H]-HSQC spectra of ferrous cyt *c*. Black trace: the H^N resonance of Q16 in the free form (~8.7 ppm). Red trace: Q16 in 1:1 complex with resting state CcP (~9.1 ppm). The solid line represents a Lorentzian fit of the resonance in the bound state. The line width (Hz) at half-height for the respective forms is denoted. (B) Overlay of part of the [^{15}N,^{1}H]-HSQC spectra of yeast ferrous cyt *c* in the free form (black) and bound to resting state CcP (red). The cyt *c*:CcP ratio was 1:1 with protein concentrations of 0.5 mM in 20 mM sodium phosphate, pH 6.0, $I = 100$ mM (NaCl), 313 K. (C) Example of a titration curve for the titration of ^{15}N ferrous cyt *c* to resting state CcP. The chemical shift changes ($\Delta\delta$) for the ^{1}H of F82 are plotted as a function of the cyt *c* to CcP ratio and fitted (*43*) with a binding constant of 5×10^5 M^{-1}.

toward the rear of the ferric protein, all chemical shift changes map onto the 10's, 20's, 70's, and 80's helices. Furthermore, the largest $\Delta\delta_{binding}$ for both oxidation states of cyt *c* occurs for residues surrounding the exposed heme edge. Therefore, for both ferrous and ferric cyt *c* the chemical shift mapping of the affected amides is in good agreement with the interface observed in the crystal structure. However, for ferric cyt *c* there is a noticeable increase in the number of amides affected, and also the magnitude of the $\Delta\delta_{binding}$ has increased (see Figure 4B). An important difference between oxidized and reduced cyt *c* is the fact that the former is paramagnetic. Therefore, we investigated the possibility that the more extensive chemical shift perturbations in the oxidized protein arise from a change in orientation of the magnetic susceptibility tensor between free and bound forms.

Magnetic Susceptibility Tensor Determination of Free and Bound Cyt c. In paramagnetic proteins such as ferric cyt *c* ($S = {}^1/_2$) the observed chemical shift is described by

$$\delta_{obs} = \delta_{dm} + \delta_{pm}$$

where δ_{obs}, δ_{dm}, and δ_{pm} are the observed, diamagnetic, and paramagnetic shifts, respectively. The paramagnetic shift arises from two contributions: (1) the Fermi contact shift associated with spin density delocalization along chemical bonds and (2) the pseudocontact effect which arises from the dipole−dipole interaction between a nucleus in space and the unpaired electron at the metal center. For nuclei that are not scalar coupled to the paramagnetic center, δ_{pm} reduces to the pseudocontact effect and is described by eq 3. Thus a change in the orientation of the magnetic susceptibility tensor of cyt *c* arising from perturbation of the surface upon binding to CcP may explain both the increase in the size of $\Delta\delta_{binding}$ and the additional residues affected.

The magnetic axes for both free and bound ferric cyt *c* were determined by performing a five-parameter least squares search for $\Delta\chi_{ax}$, $\Delta\chi_{rh}$, and $\Gamma(\alpha, \beta, \gamma)$ that minimizes the error function described in eq 5. From the NMR data sets of ferric and ferrous cyt *c* the following residues were removed: 4 prolines (25, 30, 71, 76); 8 residues with possible contact contribution to the observed paramagnetic shift (13, 14, 15, 16, 17, 18, 19, 80); 8 with reported structural changes upon oxidation/reduction (29, 39, 41, 43, 51, 60, 79, 81) (*45*); and 11 residues for which assignments are missing in either the free or the 1:1 bound form (−5, −4, 3, 4, 9, 11, 26, 33, 83, 84, 85). From the resulting set of 77 amides, which are all beyond 7 Å from the iron, four sets of inputs were derived. Set A contained the full set of 77H^N and 77N values and set B solely the 77N values. In set C the N data were omitted, and for set D the N data along with protons not within a 14 Å distance range from the Fe were left out. For both data sets (bound and free cyt *c*) fitting was performed on coordinates of two crystal structures of cyt *c*, the crystal structure of the free protein (1YCC), and the crystal structure of the complex of CcP and cyt *c* (2PCC). Fitting with either the complete set of 77H^N and 77N inputs (set A) or the 77N values (set B) resulted in a poor quality of fit judging from the error function $F/(n - 5)$ obtained (Table 2 and Figure 6A). The inadequacy of N nuclei as inputs for calculations of the magnetic tensor in an analogous way to protons has been previously noted (*46*, *47*). For this reason the N inputs were omitted in sets C and D. Both sets give identical results, with similar $F/(n - 5)$ values (Table 2) indicating that all H^N beyond 7 Å from the Fe can be used reliably for the calculation of the magnetic susceptibility tensor. In Figure 6, calculated vs observed shifts are plotted to illustrate the quality of the fits for different data sets. Comparison of the χ-tensor components from the fitting procedures for the free

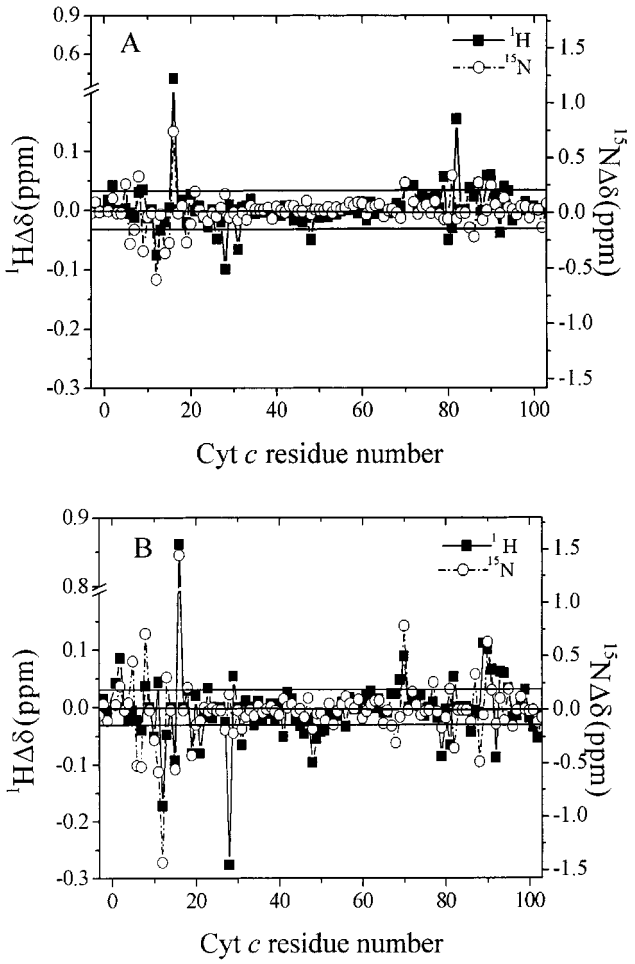

FIGURE 4: $\Delta\delta_{binding}$ (ppm) for ^{15}N and ^{1}H nuclei for (A) ferrous and (B) ferric yeast cyt *c* upon interaction with resting state CcP at equimolar concentrations. The horizontal lines at ^{1}H = 0.03 ppm indicate significance levels for protons. The levels for ^{15}N are at 0.1 ppm significance.

and bound data input sets for 1YCC shows that the orientation of the tensor is the same within error. The same is observed for the fitting on 2PCC. From these data it is concluded that no change in χ tensor is observed within error for cyt *c* upon interaction with CcP. It should be noted that the size ($\Delta\chi_{ax}$) and orientation (β, κ) differ significantly between the fittings using 1YCC and those using 2PCC as crystal structure input, independent of which NMR data set is used (free or bound cyt *c*). This indicates that the *precision* of the tensor calculations is high and that the crystal structure is the limiting factor in the *accuracy* of the calculated χ tensor.

DISCUSSION

Previous homonuclear NMR experiments on the transient complex formed between cyt *c* and CcP have identified a number of protons belonging to cyt *c* amino acid residues which are affected upon complex formation (*25*, *30*). Additionally, hyperfine-shifted signals of cyt *c* heme protons also demonstrate sizable chemical shift changes upon interaction (*24*−*26*). In this work, by labeling yeast cyt *c* with ^{15}N, a qualitative picture of the binding site on cyt *c* has been obtained, indicating that the interaction site in solution is similar to the one in the crystals. Furthermore, distinct differences between the ferrous and ferric forms of

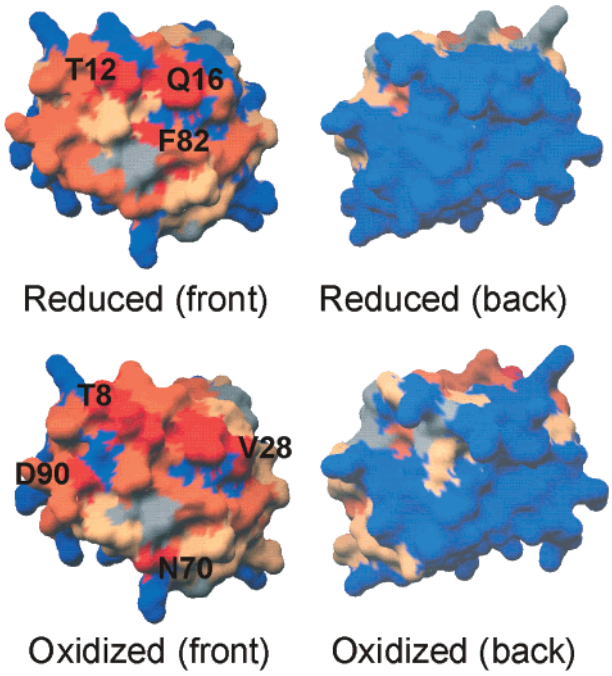

FIGURE 5: Surface representations of cyt *c* drawn using GRASP v.1.3 (*44*) with each residue colored according to the largest $\Delta\delta_{binding}$ observed for its backbone amide in the presence and absence of equimolar resting state CcP. The color scheme is given in Table 1.

Table 1: Classification of ^{15}N, ^{1}H Chemical Shift Changes for Ferrous and Ferric Cyt *c* upon Complex Formation with Resting State CcP (I = 100 mM, pH 6.0, 313 K)

				no. of residues	
category	^{1}H size (ppm)	^{15}N size (ppm)	residue color in Figure 5	ferrous cyt *c*	ferric cyt *c*
A	prolines/ unassigned	prolines/ unassigned	gray	4 5	4 6
B	≤0.03	≤0.1	blue	65	42
C	≤0.06	≤0.3	cream	15	30
D	≤0.10	≤0.6	orange	16	20
E	≤1.00	≤2.0	red	3	6

cyt *c* are observed in the size of the affected surface area (Figure 5). Although no side chain information is obtained from this technique, a recent homonuclear NMR study between the complex of cytochrome *f* and plastocyanin (*48*) has shown the binding interface on plastocyanin to be in good agreement with the one previously determined using the ^{15}N labeling method (*13*).

In the crystal structure of the complex the only structural change observed for cyt *c* is the reorientation of the Gln16 side chain to form a H-bond with its backbone amide (*4*). This structural change was interpreted not to be due to complex formation but to the conditions under which the crystals were grown (*4*). For both ferrous and ferric cyt *c*, Gln16 exhibits the largest ^{1}H $\Delta\delta_{binding}$ with the cross-peak in the spectra moving to a lower field by 0.41 ppm for the reduced (Figure 3) and 0.8 ppm for the oxidized protein. Wagner et al. report the observation that chemical shifts for amide protons move to a lower field with decreasing H-bond lengths (*49*). This suggests that the reorientation of the Gln16 side chain in the crystal structure is not an artifact arising from the conditions used to grow the crystals but is indeed a structural change upon complex formation in both oxidation states of cyt *c*.

Table 2: Calculated Angles and Components of the Magnetic Susceptibility Tensor of Ferric Cyt *c* in the Free Form and Bound to Resting State CcP, with the Numbers in Parentheses Indicating the Error from the Five-Parameter Fitting Procedure

X-ray coordinates	NMR data	atom set[a]	α (deg)	β (deg)	κ (deg)	$\Delta\chi_{ax}$[b]	$\Delta\chi_{rh}$[b]	$F/(n-5)$ (ppm^2)
1YCC	free cyt *c*	$77H^N + 77N$ (A)	28 (36)	5 (4)	166 (19)	2.00 (0.19)	−0.45 (0.35)	0.314
2PCC	free cyt *c*	$77H^N + 77N$ (A)	36 (13)	13 (4)	161 (16)	2.05 (0.20)	−0.51 (0.34)	0.317
1YCC	free cyt *c*	77N (B)	358 (360)	0 (6)	334 (40)	2.24 (0.35)	−0.40 (0.67)	0.57
1YCC	free cyt *c*	$77H^N$ (C)	28 (4)	11 (1)	−5 (3)	1.81 (0.04)	−0.62 (0.07)	0.007
1YCC	bound cyt *c*	$77H^N$ (C)	29 (4)	11 (1)	−5 (3)	1.77 (0.04)	−0.64 (0.06)	0.006
2PCC	free cyt *c*	$77H^N$ (C)	31 (3)	17 (1)	−12 (3)	1.90 (0.05)	−0.65 (0.08)	0.009
2PCC	bound cyt *c*	$77H^N$ (C)	31 (3)	17 (1)	−12 (3)	1.85 (0.04)	−0.66 (0.07)	0.007
1YCC	free cyt *c*	$37H^N$ (D)	31 (5)	11 (1)	−7 (4)	1.84 (0.05)	−0.67 (0.10)	0.009
1YCC	bound cyt *c*	$37H^N$ (D)	32(5)	11 (1)	−7 (3)	1.78 (0.04)	−0.68 (0.08)	0.007
2PCC	free cyt *c*	$39H^N$ (D)	32 (3)	17 (1)	−13 (4)	1.93 (0.06)	−0.70 (0.11)	0.012
2PCC	bound cyt *c*	$39H^N$ (D)	32 (3)	17 (1)	−13 (3)	1.89 (0.05)	−0.70 (0.10)	0.009

[a] (A), (B), and (C) ≥7 Å distance from the Fe center. (D) 7−14 Å from the Fe center. [b] Axial and rhombic anisotropies have the units 10^{-8} m^3/mol.

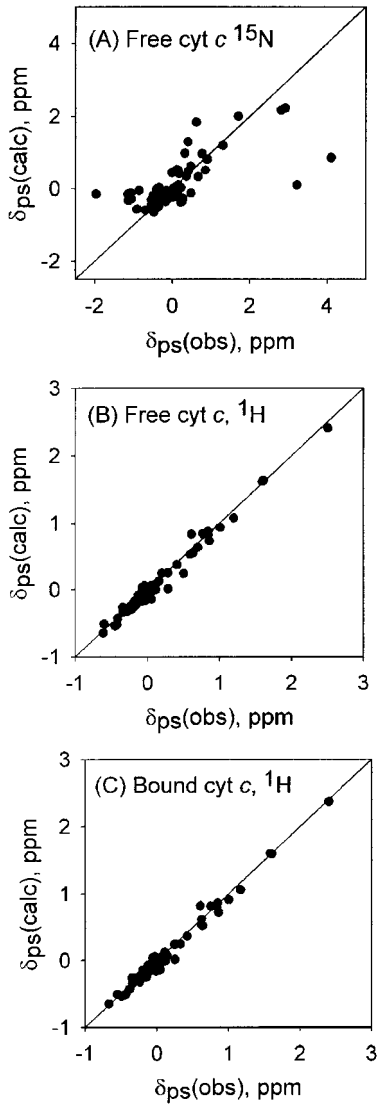

FIGURE 6: Plot of δ_{ps}(obs) vs δ_{ps}(calc) at 313 K for the optimized magnetic axes obtained from a five-parameter least squares search for $\Gamma(\alpha, \beta, \gamma)$ and $\Delta\chi$s using eq 3 for (A) ^{15}N nuclei with 77 N (set B) inputs for free cyt *c*, (B) ^{1}H nuclei with $77H^N$ inputs (set C) for free cyt *c*, and (C) ^{1}H nuclei with $77H^N$ inputs (set D) for bound cyt *c*, all fitted on 1YCC. The solid lines correspond to a perfect fit.

In addition to Gln16, Thr12 and Phe82 (Figure 1) are also categorized in group E of Table 1 for the ferrous protein. As with Gln16, Phe82 has been implicated to undergo a structural change upon complex formation (*26*), although not observed in the crystal structure. Thr12 has not been cited in structural studies before, but the side chain is within 3 Å and the amide is 5 Å from the surface of CcP in the crystal structure. All three residues sit around the exposed heme edge, with Thr12 and Gln16 above and Phe82 below (Figure 5). The large $\Delta\delta_{binding}$ implies a change of the chemical environment most likely caused by prominent interactions of this triad with the surface of CcP or as a possible consequence of subtle structural rearrangements. The latter is attractive in terms of an ET mechanism and has been discussed previously in terms of increasing exposure of pyrrole ring B to the solvent by side chain movement of nearby residues (*4*, *30*). The aforementioned residues are all within the vicinity of pyrrole ring B.

For ferric cyt *c* the largest $\Delta\delta_{binding}$ is again for residues surrounding the exposed heme edge, with hydrophobic residues such as Phe10, Val28, Phe82, and Ala81 seemingly playing a significant role in binding (Table S2). Overall, the affected residues on the front face of the protein are the same in both oxidized and reduced forms. However, differences in data compared to the ferrous form are apparent. First, the size of the $\Delta\delta_{binding}$ has increased (Figure 4B), and, second, the number of amides affected has increased to 56. The latter is appreciated in Figure 5, where the major affects are assigned to the front face, but in addition chemical shift changes for amides are now observed for residues toward the side and rear of the protein. An interesting structural difference between the two oxidation states of cyt *c* is the rearrangement of the propionate-7 substituent in the oxidized protein (*50*), which results in the formation of a new H-bond to the amide of Gly41. Homonuclear experiments on the complex indicate that the side chain protons of propionate-7 experience a chemical shift change upon binding (*27*). This explains the observation that Gly41 exhibits a significant chemical shift change in the complex of oxidized cyt *c* (^{1}H −0.05 and ^{15}N 0.1 ppm) but not for the reduced protein.

To establish whether a change in the cyt *c* χ tensor upon complex formation could be the cause of the additional changes observed in the oxidized form, the size and orientation of the χ tensor were determined in both the bound and free form. An earlier study (*30*) had reported such a change in tensor on the basis of magnetic axes calculations with small sets of pseudocontact shifts. In this study (*30*), a

different crystal structure was used to calculate the tensor in the bound (2PCC) than in the free form (1YCC). Our results, based on much larger input sets, indicate that the tensor is not affected significantly by complex formation. It also shows that the use of the two crystal structures results in differences in the β and κ angles of the calculated χ tensors, similar to those found in ref *30*. A number of χ-tensor components of various cytochrome *c* species have previously been reported (*30*, *39*, *45*, *50*−*52*). On the basis of the solution structure of yeast cyt *c*, Banci et al. (*50*) report $\Delta\chi_{ax} = 1.34 \times 10^{-8}$ m^3/mol and $\Delta\chi_{rh} = -0.63 \times 10^{-8}$ m^3/mol. The axial component obtained from their fittings is significantly lower than observed here ($\Delta\chi_{ax} = 1.81 \times 10^{-8}$ m^3/mol), with our value being closer to the EPR-reported *g*-value, $g_{ax} = 1.80 \times 10^{-8}$ m^3/mol (*45*). However, as we have shown, different sizes ($\Delta\chi$s) and angles (α, β, κ) are obtained depending on which structure is used for the calculations. Indeed, Banci et al. (*50*) point out that discrepancies arise between the X-ray and solution structure of yeast cyt *c* because the solution structure is calculated with the inclusion of pseudocontact restraints.

As a change in χ tensor is not the reason for the observed differences between oxidized and reduced cyt *c*, two alternative explanations can be proposed to explain this phenomenon. First, the differences may arise due to a change in the binding mode of oxidized cyt *c* compared to the reduced form. In both cases the chemical shift perturbations are relatively large, suggesting that they represent a single orientation of cyt *c* in the complex. However, taking into account the dynamic nature of the complex (*20*−*23*), this orientation may be in fast equilibrium with a set of "loose" orientations, as also suggested for the complex of cytochrome *f* and plastocyanin (*13*):

$$\text{cyt } c + \text{CcP} \rightleftharpoons \{\text{cyt } c\text{:CcP}\} \rightleftharpoons \text{cyt } c\text{:CcP*}$$

where {cyt *c*:CcP} represents an encounter complex with an ensemble of orientations and cyt *c*:CcP* is the complex in a single orientation observed by NMR. Multiple loose orientations, stabilized mainly by electrostatic interactions, are expected to be invisible by the chemical shift perturbation method, since the chemical shift changes are very small in these complexes (*43*). If oxidized cyt *c* exhibits a somewhat different and stronger interaction in cyt *c*:CcP*, pulling the equilibrium more toward the single orientation, this would explain the larger and more extensive chemical shift changes.

The second explanation is related to structural and dynamic differences between the two oxidation states. It could be that in the more flexible structure of the oxidized protein (*36*, *50*) secondary structure elements can move more easily relative to each other. This allows for the binding effects at the interface to be relayed to other parts of the protein (i.e., 40's, 50's, 60's, 90's helices) via a concerted movement of a helix or loop. This will affect the chemical shifts of (H-bonded) amides in particular, as these are very sensitive to structural changes (*53*−*55*). Extensive changes away from the binding site have also been observed in hydrogen/deuterium exchange experiments with ferric cyt *c* (*29*). In these studies exchange behavior of individual backbone amide protons was investigated for cyt *c* in both the free and bound forms. The largest amide protection factors were found in the 10's and 70's helices (front face), but in addition high amide protection factors were observed for residues 59 and 60 and the 90's helix, to the rear of the protein. Both explanations are not mutually exclusive, and further research aimed at determining the structure of the complex in solution may be able to elucidate this problem.

ACKNOWLEDGMENT

We thank Professors A. G. Mauk and B. M. Hoffman for the cyt *c* and CcP expression plasmids, respectively. Dr. V. Leesch is acknowledged for help with CcP expression, Professor G. N. LaMar for the use of his suite of programs for the magnetic axes calculations, and C. Erkelens for assistance with NMR.

SUPPORTING INFORMATION AVAILABLE

Two tables listing significant chemical shift changes upon 1:1 interaction with resting state CcP for reduced and oxidized cyt *c*, respectively. This material is available free of charge via the Internet at http://pubs.acs.org.

REFERENCES

1. Sheinerman, F. B., Norel, R., and Honig, B. (2000) *Curr. Opin. Struct. Biol. 10*, 153−159.
2. McLendon, G. (1991) *Struct. Bonding 75*, 159−174.
3. Bendall, D. S. (1996) in *Protein Electron Transfer* (Bendall, D. S., Ed.) pp 43−68, BIOS Scientific Publishers, Oxford.
4. Pelletier, H., and Kraut, J. (1992) *Science 258*, 1748−1755.
5. Chen, L., Durley, R. C., Poliks, B. J., Hamada, K., Chen, Z., Mathews, F. S., Davidson, V. L., Satow, Y., Huizinga, E., and Vellieux, F. M. (1992) *Biochemistry 31*, 4959−4964.
6. Chen, L., Durley, R. C., Mathews, F. S., and Davidson, V. L. (1994) *Science 264*, 86−90.
7. Sevrioukova, I. F., Li, H., Zhang, H., Peterson, J. A., and Poulos, T. (1999) *Proc. Natl. Acad. Sci. U.S.A. 96*, 1863−1868.
8. Kurisu, G., Kusunoki, M., Katoh, E., Yamazaki, T., Teshima, K., Onda, Y., Kimata-Ariga, Y., and Hase, T. (2001) *Nat. Struct. Biol. 8*, 117−121.
9. Müller, J. J., Lapko, A., Bourenkov, G., Ruckpaul, K., and Heinemann, U. (2001) *J. Biol. Chem. 276*, 2786−2789.
10. Bertini, I., and Luchinat, C. (1999) *Curr. Opin. Chem. Biol. 3*, 145−151.
11. Guiles, R. D., Sarma, S., Di Gate, R. J., Banville, D., Basus, V. J., Kuntz, I. D., and Waskell, L. (1996) *Nat. Struct. Biol. 3*, 333−339.
12. Morelli, X., Dolla, A., Czjzek, M., Nuno Palma, P., Blasco, F., Krippahl, L., Moura, J. J. G., and Guerlesquin, F. (2000) *Biochemistry 39*, 2530−2537.
13. Ubbink, M., Ejdeback, M., Karlsson, B. G., and Bendall, D. S. (1998) *Structure 6*, 323−335.
14. Nocek, J. M., Zhou, J. S., DeForest, S., Priyadarshy, S., Beratan, D. N., Onuchic, J. N., and Hoffman, B. M. (1996) *Chem. Rev. 96*, 2459−2489.
15. Kraulis, P. J. (1991) *J. Appl. Crystallogr. 24*, 946−950.
16. Poulos, T. L., and Kraut, J. (1980) *J. Biol. Chem. 255*, 10320−10330.
17. Zhou, J. S., and Hoffman, B. M. (1994) *Science 265*, 1693−1696.
18. Zhou, J. S., Nocek, J. M., DeVan, M. L., and Hoffman, B. M. (1995) *Science 269*, 204−207.
19. Leesch, V. W., Bujons, J., Mauk, A. G., and Hoffman, B. M. (2000) *Biochemistry 39*, 10132−10139.
20. Northrup, S. H., Boles, J. O., and Reynolds, J. C. L. (1988) *Science 241*, 67−70.
21. Hazzard, J. T., Moench, S. J., Erman, J. E., Satterlee, J. D., and Tollin, G. (1988) *Biochemistry 27*, 2002−2008.
22. Hazzard, J. T., McLendon, G., Cusanovich, M. A., Das, G., Sherman, F., and Tollin, G. (1988) *Biochemistry 27*, 4445−4451.

23. Stemp, E. D. A., and Hoffman, B. M. (1993) *Biochemistry 32*, 10848−10865.
24. Satterlee, J. D., Moench, S. J., and Erman, J. E., (1987) *Biochim. Biophys. Acta 912*, 87−97.
25. Moench, S. J., Chroni, S., Lou, B.-S., Erman, J. E., and Satterlee, J. D. (1992) *Biochemistry 31*, 3661−3670.
26. Yi, Q., Erman, J. E., and Satterlee, J. D. (1992) *J. Am. Chem. Soc. 114*, 7907−7909.
27. Yi, Q., Erman, J. E., and Satterlee, J. D. (1994) *J. Am. Chem. Soc. 116*, 1981−1987.
28. Jeng, M. F., Englander, S. W., Pardue, K., Rogalskyj, J. S., and McLendon, G. (1994) *Nat. Struct. Biol. 1*, 234−238.
29. Yi, Q., Erman, J. E., and Satterlee, J. D. (1994) *Biochemistry 33*, 12032−12041.
30. Sukits, S. F., Erman, J. E., and Satterlee, J. D. (1997) *Biochemistry 36*, 5251−5259.
31. Pollock, W. B. R., Rosell, F. I., Twitchett, M. B., Dumont, M. E., and Mauk, A. G. (1998) *Biochemistry 37*, 6124−6131.
32. Morar, A. S., Kakouras, D., Young, G. B., Boyd, J., and Peilak, G. J. (1999) *J. Biol. Inorg. Chem. 4*, 220−222.
33. Goodin, D. B., Davidson, M. G., Roe, J. A., Mauk, A. G., and Smith, M. (1991) *Biochemistry 30*, 4953−4962.
34. Vitello, L. B., Huang, M., and Erman, J. E. (1990) *Biochemistry 29*, 4283−4288.
35. Gao, Y., Boyd, J., Williams, R. J. P., and Pielak, G. J. (1990) *Biochemistry 29*, 6994−7003.
36. Fetrow, J. S., and Baxter, S. (1999) *Biochemistry 38*, 4480−4492.
37. Kraulis, P. J. (1989) *J. Magn. Reson. 84*, 627−633.
38. Kraulis, P. J., Domaille, P. J., Campbell-Burk, S. L., Van Aken, T., and Laue, E. D. (1994) *Biochemistry 33*, 3515−3531.
39. Williams, G., Clayden, N. J., Moore, G. R., and Williams, R. J. P. (1985) *J. Mol. Biol. 183*, 447−460.
40. Emerson, S. D., and LaMar, G. N. (1990) *Biochemistry 29*, 1556−1566.
41. Louie, G. V., and Brayer, G. D. (1990) *J. Mol. Biol. 214*, 527−555.
42. Koradi, R., Billeter, M., and Wüthrich, K. (1996) *J. Mol. Graphics 14*, 51−55.
43. Ubbink, M., and Bendall, D. S. (1997) *Biochemistry 36*, 6326−6335.
44. Nicholls, A., Sharp, K., and Honig, B. (1991) *Proteins: Struct., Funct., Genet. 11*, 281−296.
45. Gao, Y., Boyd, J., Pielak, G. J., and Williams, R. J. P. (1991) *Biochemistry 30*, 1928−1934.
46. Boyd, J., Dobson, C. M., Morar, A. S., Williams, R. J. P., and Pielak, G. J. (1999) *J. Am. Chem. Soc. 121*, 9247−9248.
47. Tsan, P., Caffrey, M., Daku, M. L., Cusanovich, M., Marion, D., and Gans, P. (1999) *J. Am. Chem. Soc. 121*, 1795−1805.
48. Ejdebäck, M., Bergkvist, A., Karlsson, B. G., and Ubbink, M. (2000) *Biochemistry 39*, 5022−5027.
49. Wagner, G., Pardi, A., and Wüthrich, K. (1983) *J. Am. Chem. Soc. 105*, 5948−5949.
50. Banci, L., Bertini, I., Bren, L., Gray, H. B., Sompornpisut, P., and Turano, P. (1997) *Biochemistry 36*, 8992−9001.
51. Feng, Y., Roder, H., and Englander, S. W. (1990) *Biochemistry 29*, 3494−3504.
52. Banci, L., Bertini, I., Gray, H. B., Luchinat, C., Reddig, T., Rosato, A., and Turano, P. (1997) *Biochemistry 36*, 9867−9877.
53. DeDios, A. C., Pearson, J. G., and Oldfield, E. (1993) *Science 260*, 1491−1496.
54. Facelli, J. C., Pugmire, R. J., and Grant, D. M. (1996) *J. Am. Chem. Soc. 118*, 5488−5489.
55. Walling, A. E., Pargas, R. E., and deDios, A. C. (1997) *J. Phys. Chem. 101*, 7299−7303.

BI0025823